

Possibility of Observing Spiral Scattering of Relativistic Particles in a Bent Crystal

G. V. Kovalev

North Saint Paul, MN 55109, USA

(Dated: Dec. 26, 2008)

The peak position, impact-parameter range, and optimal conditions for observing spiral scattering of relativistic particles in a uniformly bent crystal are estimated. The existence of spiral scattering with a square-root singularity is pointed out. In this case, the secondary process of volume capture to the channeling mode is absent and the conditions for observing this effect are most favorable.

PACS numbers: 03.65.Ge; 03.65.Fd; 03.65.; 03.65.Db; 02.30.Em

The phenomenon of spiral scattering occurs due to the appearance of a negative logarithmic singularity of the classical deflection function $\chi(b)$ of a particle or light ray for a certain impact parameter $b = b_s$ [1]. Resonance scattering is a quantum mechanical analog of spiral scattering [2]. However, resonance scattering includes a wider class of quantum-mechanical phenomena. In particular, it can appear in the scattering of fast particles by a cylindrical well (see, e.g., [3]), whereas classical spiral scattering by such a potential is absent [4].

To illustrate this feature and determine the spiral-scattering boundaries, let us compare scattering by a cylindrical or spherical potential well of radius R and depth $-U_0$ and scattering by a well of the same depth and radius, but with a smoothed parabolic edge of width $d/2$ ($d \ll R$) (curves 1 and 2, respectively, in Fig. 1a):

$$U(r) = -U_0 \frac{4}{d^2} \begin{cases} 0, & R < r; \\ (r - R)^2, & (R - \frac{d}{2}) < r < R; \\ \frac{d^2}{4}, & 0 < r < (R - \frac{d}{2}). \end{cases} \quad (1)$$

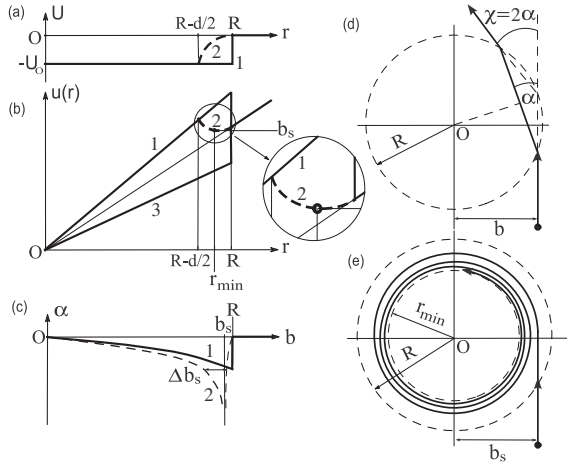


FIG. 1: (a) Square-well potential shown by solid curve 1 and a smoothed well given by dashed curve 2. (b) The function $u(r)$ given by Eq. (3) for the (line 1) well, (line 2) smoothed well, and (line 3) barrier. (c) The deflection function $\alpha = \chi/2$. (d) The trajectory of a particle in the square well. (e) The spiral trajectory of a particle in the smoothed square well.

The classical deflection function

$$\chi(b) = 2\alpha(b) = \pi - 2b \int_{r_0}^{\infty} \frac{dr}{r \sqrt{r^2 [1 - \phi(r)] - b^2}}, \quad (2)$$

where $\phi(r) = 2U(r)E/(p_{\infty}^2 c^2)$ and $b, U(r), E, p_{\infty}$ are the impact parameter, centrally symmetric potential, total energy, and momentum of a particle at infinity, respectively, can be calculated for both cases, but the absence of spiral scattering for a square well can be seen directly in the plot (curve 1 in Fig. 1b) of the function

$$u(r) = r \sqrt{1 - \phi(r)}, \quad (3)$$

which has a finite step and a local minimum for $r = R$. Therefore, the derivative $u(R)'$ is indeterminate at this point. Deflection function (2) is expressed in terms of function (3) as

$$\chi(b) = \pi - 2b \int_{r_0}^{\infty} \frac{dr}{r \sqrt{u(r) - b \sqrt{u(r) + b}}}, \quad (4)$$

where, as before, the turning point r_0 is determined from the equation $u(r_0) = b$. In the case of the smoothed potential (curve 2), the function $u(r)$ has a smooth local minimum at the point r_{min} , at which $u'(r_{min}) = 0$. If the impact parameter coincides with this minimum, i.e.,

$$b_s = u(r_{min}), \quad (5)$$

both the radial velocity and radial acceleration of the particle become zero (for more detail, see [1, 5]) and the conditions for spiral scattering are implemented. Here, the function $u(r)$ in the vicinity of the minimum r_{min} is represented in the form

$$u(r) \approx u(r_{min}) + \frac{u''(r_{min})}{2} (r - r_{min})^2, \quad (6)$$

while the local-minimum point r_{min} determined from the condition $u'(r_{min}) = 0$ is specified by the equation

$$1 - \phi(r_{min}) - \frac{r_{min}}{2} \phi'(r_{min}) = 0. \quad (7)$$

This equation holds for any potential; for Eq. (1), it reduces to the simple form

$$2\hat{r}_{min}^2 - 3\hat{r}_{min} + 1 + \delta = 0. \quad (8)$$

Here,

$$\hat{r} = \frac{r}{R}, \quad \hat{d} = \frac{d}{R}, \quad \delta = \frac{\hat{d}^2}{4|\phi_o|}, \quad \phi_o = \frac{-2U_0E}{p_\infty^2 c^2} \quad (9)$$

and $L = \sqrt{|\phi_o|}$ is the Lindhard channeling angle. In the case of the potential given by Eq. (1), semi-channeling can occur when a particle moves near the potential edge and is successively reflected from its inner wall. Hereafter, a quantity with the symbol $\hat{\cdot}$ denotes the corresponding quantity without this symbol divided by R .

Only one, physically meaningful, of the two solutions of Eq. (8) with the plus sign of the square root should be retained:

$$\hat{r}_{min} = \frac{3}{4} + \frac{\sqrt{1-8\delta}}{4}. \quad (10)$$

Note the important condition that should be in the range $1 - \hat{d}/2 \leq \hat{r}_{min} \leq 1$ (see Fig. 1); otherwise, the local minimum does not exist. The lower boundary $1 - \hat{d}/2 = \hat{r}_{min}$ substituted into the left-hand part of Eq. (10) yields the critical parameter δ_c for the observation of the spiral scattering of relativistic particles by a smoothed well:

$$\delta \leq \delta_c = \frac{\hat{d}(1-\hat{d})}{2}. \quad (11)$$

Since, according to Eq. (9), $|\phi_o| = \frac{\hat{d}^2}{4\delta}$, the corresponding criterion for the squared Lindhard angle $|\phi_{o,c}|$ can also be written as

$$|\phi_o| \geq |\phi_{o,c}| = \frac{\hat{d}}{2(1-\hat{d})}. \quad (12)$$

Next, since the smooth-edge region is small, $\hat{d} \ll 1$ (or $d \ll R$), Eqs. (11) and (12) reduce to the inequalities $\delta \leq \hat{d}/2$, $|\phi_o| \geq \hat{d}/2$, respectively. It is easy to see that these constraints are equivalent to the criterion $R \geq R_c = p_\infty^2 c^2 d / (4U_0E) = d / (2\theta_L^2)$. It was noted in [4, 5] that this criterion is equivalent to the Tsyganov criterion for the existence of the channeling effect in a bent crystal. Since $\hat{d} \ll 1$, $\delta \ll 1$ and Eq. (10) can be approximately written as $\hat{r}_{min} \cong 1 - \delta$.

For comparison, the quantity $\alpha(\hat{b}) = \chi(\hat{b})/2$ for the square well in the range $0 \leq \hat{b} \leq 1$ is given by the expression (see Section 19 in [6] or Eq. (12) in [5])

$$\alpha(\hat{b}) = \arcsin\left(\frac{\hat{b}(\sqrt{1-\hat{b}^2} - \sqrt{1-\phi_o-\hat{b}^2})}{\sqrt{1-\phi_o}}\right). \quad (13)$$

This corresponds to curve 1 in Fig. 1c. All deflection angles for the square well are negative with the maximum absolute value

$$|\alpha(1)| = \arcsin\left(\frac{\sqrt{-\phi_o}}{\sqrt{1-\phi_o}}\right), \quad (14)$$

achieved near the well edge $\hat{b} = 1$. Under the condition $\sqrt{|\phi_o|} \ll 1$, this angle is $|\alpha(1)| \approx \theta_L$. A typical trajectory of particles in such a potential is shown in Fig. 1d. In the case of the smoothed well given by Eq. (1), deflection function (2) is given by a lengthy formula with elliptical functions. However, if approximation (6) is used, the deflection function for the impact parameters $\hat{b}_s < \hat{b} < 1$ takes the form

$$\alpha(\hat{b}) = \frac{\pi}{2} - \arcsin(\hat{b}) - \sqrt{\frac{\hat{b}}{\hat{u}(\hat{r}_{min})''}} * \frac{\ln\left(\frac{2(\hat{r}_0 - \hat{r}_{min})}{(\sqrt{\hat{r}_0(1+\hat{r}_0-2\hat{r}_{min})} - \sqrt{(1-\hat{r}_0)(2\hat{r}_{min}-\hat{r}_0)})^2}\right)}{\sqrt{\hat{r}_{min}^2 - (\hat{r}_0 - \hat{r}_{min})^2}}, \quad (15)$$

where $\hat{r}_0 = \hat{r}_{min} + \sqrt{2(\hat{b} - \hat{u}(\hat{r}_{min}))/\hat{u}(\hat{r}_{min})''}$. The deflection function for the impact parameters $0 < \hat{b} < \hat{b}_s$ has the different form

$$\alpha(\hat{b}) = \arcsin\left(\frac{\hat{b}}{A\sqrt{1+\hat{d}^2/(4\delta)}}\right) - \arcsin(\hat{b}) - \sqrt{\frac{\hat{b}}{C\hat{u}(\hat{r}_{min})''}} \ln\left(\frac{2C + AB + 2\sqrt{C}\sqrt{A^2 + AB + C}}{A(2C + B + 2\sqrt{C}\sqrt{1+B+C})}\right), \quad (16)$$

where $A = 1 - \hat{d}/2$, $B = -2\hat{r}_{min}$, $C = \hat{r}_{min}^2 + 2(\hat{u}(\hat{r}_{min}) - \hat{b})/(\hat{u}(\hat{r}_{min})'')$.

If $\hat{b} \rightarrow \hat{b}_s = \hat{u}(\hat{r}_{min})$, the deflection angles given by Eqs. (15) and (16) tend logarithmically to $-\infty$ (see curve 2 in Fig. 1c); i.e., the particle orbits the potential center by an angle exceeding maximum angle (14) for a square well. Under the condition $\hat{b} = \hat{b}_s$, spiral scattering appears; in this case, the relativistic particle does not have the outgoing branch and is located near the potential for an infinitely long time (see Fig. 1e) approaching the limit cycle $\hat{r} \rightarrow \hat{r}_{min}$. Only one trajectory satisfies the spiral-scattering criterion. Trajectories with impact parameters close to \hat{b}_s have the usual ingoing and outgoing branches, but can follow the circle over an angle exceeding the Lindhard angle (14).

Let the spiral-scattering range be defined as the impact-parameter range Δb_s near $b = b_s$, in which the absolute values of negative angles (15) and (16) exceed maximum angle (14) for the square well (see Fig. 1c). Such a definition is useful since it distinguishes the spiral scattering from both refraction ranging within the angle given by Eq. (14) and volume reflection, which has a positive sign [7], but does not exceed the angle given by Eq. (14). The spiral scattering is also different from channeling (see below). The substitution of Eq. (10) into Eq. (5) yields the exact value for the spiral impact parameter \hat{b}_s in the case of potential (1):

$$\hat{b}_s = \frac{3 + \sqrt{1-8\delta}}{4} \sqrt{1 + \frac{(1 - \sqrt{1-8\delta})^2}{16\delta}}. \quad (17)$$

If $\delta \ll 1/8$, $\hat{b}_s \approx 1 - \delta/2$.

The right and left boundaries of the spiral-scattering range are determined as the roots of the transcendental equation

$$\alpha(\hat{b}) = -\arcsin\left(\frac{\sqrt{|\phi_o|}}{\sqrt{1+|\phi_o|}}\right), \quad (18)$$

with $\alpha(\hat{b})$ given by Eqs. (15) and (16), respectively. By solving the simpler transcendental equation $c_1 \ln(\Delta \hat{b}_{sr}) + c_2 = 0$ (where c_1 and c_2 are constants), which is obtained by retaining only the first terms in the expansions of all functions in Eq. (15) in the power series of $(\hat{b} - \hat{b}_s)$ in the right neighborhood of \hat{b}_s , the right part $\Delta \hat{b}_{sr} = \hat{b}_r - \hat{b}_s$ of the region $\Delta \hat{b}_s$ is determined in the form

$$\Delta \hat{b}_{sr} = 2\hat{u}(\hat{r}_{min})'' \delta^2 \exp\left(-\sqrt{\frac{\hat{u}(\hat{r}_{min})''}{\hat{b}_s}} * \left(\frac{\hat{d}}{\sqrt{\delta}} + 2\sqrt{1 - \hat{b}_s^2}\right)\right). \quad (19)$$

Hereafter, it is taken into account the conditions $|\phi_o| \ll 1$ and $\delta \ll 1/8$, which are certainly valid in the relativistic case.

To calculate the left-hand part $\Delta \hat{b}_{sl} = \hat{b}_s - \hat{b}_l$ in the entire range given by Eq. (12), it is necessary to retain a few terms in the expansion of Eq. (16) in the power series of $(\hat{b} - \hat{b}_s)$, since the impact parameter \hat{b}_s approaches the inflection point $\approx \hat{d}/4$ of the function $\hat{u}(\hat{r})$ with a variation in the parameter $|\phi_o|$. In the case where they are kept, the solution of the transcendental equation $c_1 \ln(c_3 \Delta \hat{b}_{sl}) + \Delta \hat{b}_{sl} + c_2 = 0$, obtained by retaining only first two terms in the series, has a solution expressed in terms of the Lambert function $W(x)$, which is defined through the relation $W(x) \exp W(x) = x$ [8], as

$$\Delta \hat{b}_{sl} = c_1 W\left(\frac{\exp(-\frac{c_2}{c_1})}{c_1 c_3}\right), \quad (20)$$

where the parameters c_1 , c_2 and c_3 are

$$\begin{aligned} c_1 &= \frac{\sqrt{A^2(1+\phi_0) - \hat{b}_s^2} \sqrt{1 - \hat{b}_s^2}}{(\sqrt{A^2(1+\phi_0) - \hat{b}_s^2} - \sqrt{1 - \hat{b}_s^2}) \sqrt{\hat{u}(\hat{r}_{min})''}} \\ c_2 &= -\sqrt{A^2(1+\phi_0) - \hat{b}_s^2} \sqrt{1 - \hat{b}_s^2} + \\ &+ \frac{\hat{d} \sqrt{A^2(1+\phi_0) - \hat{b}_s^2} \sqrt{1 - \hat{b}_s^2}}{2\sqrt{\delta(1+\phi_0)}(\sqrt{A^2(1+\phi_0) - \hat{b}_s^2} - \sqrt{1 - \hat{b}_s^2})} \\ c_3 &= \frac{A}{2\delta(\hat{d}/2 - \delta) \hat{u}(\hat{r}_{min})''}. \end{aligned} \quad (21)$$

The width of the impact-parameter region $\Delta \hat{b}_s$ where spiral scattering is significant is determined by the sum

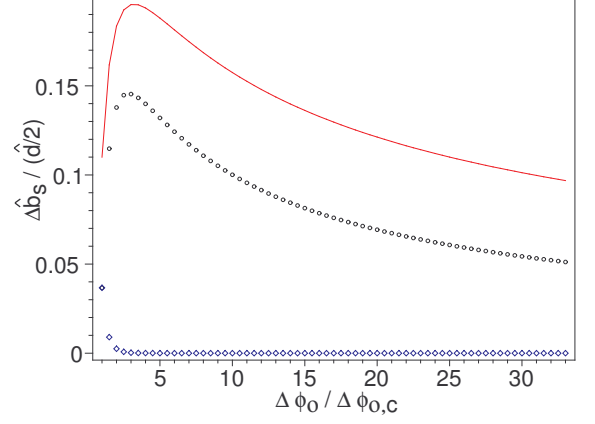


FIG. 2: Dimensionless spiral-scattering width $\Delta \hat{b}_s$ versus the parameter $|\phi_o|/|\phi_{o,c}|$. The solid curve is the numerical calculation by 18. The circles show the contribution from $\Delta \hat{b}_s$ to $\Delta \hat{b}_{sl}$, according to 20. The diamonds show the contribution from $\Delta \hat{b}_s$ to $\Delta \hat{b}_{sr}$, according to 19.

of Eqs. (19) and (20):

$$\Delta \hat{b}_s = \Delta \hat{b}_{sr} + \Delta \hat{b}_{sl}. \quad (22)$$

The second derivative $\hat{u}(\hat{r}_{min})''$ in Eqs. (19) and (20) is expressed in terms of δ as

$$\hat{u}(\hat{r}_{min})'' = \frac{4\hat{r}_{min} - 3}{\delta \sqrt{1 + \frac{(\hat{r}_{min}-1)^2}{\delta}}} = \frac{\sqrt{1-8\delta}}{\delta \sqrt{1 + \frac{(1-\sqrt{1-8\delta})^2}{16\delta}}}, \quad (23)$$

and $\hat{u}(\hat{r}_{min})'' \approx \delta^{-1}$ for small δ values.

In addition to approximate formulas (19) and (20) for the right and left boundaries of the spiral-scattering region, respectively, transcendental equations (18) were also solved numerically. The result is shown by the solid curve in Fig. 2. The numerical solution for the right-hand boundary (diamonds) coincides with high accuracy with Eq. (19). Formula (20) for the left-hand boundary (circles) provides an underestimated result, but the behavior of the curve is the same as predicted by the accurate numerical solution. In addition, the contribution from the right-hand part of the spiral-scattering range to the total width is much smaller than the contribution from the left-hand part, except for the vicinity of the critical point $|\phi_o| = |\phi_{o,c}|$. As a result, the logarithmic branches of the deflection function on the right and left sides of $b = b_s$ are not symmetric for the considered potential (curves 2 and 3 in Fig. 3).

Note an important feature of the width of the spiral-scattering region. Let the potential parameters R , U_0 , and d be fixed and the relativistic particle energy decrease so that $|\phi_o|$ increases from critical value (12) to a few tens of $|\phi_{o,c}|$ without violating the condition $|\phi_o| \ll 1$. Then, the width $\Delta \hat{b}_s$ of the spiral-scattering region increases

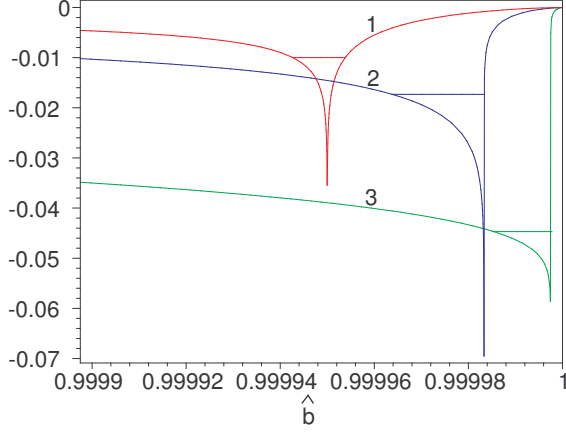


FIG. 3: Deflection function $\alpha(\hat{b})$ for the potential given by 1: $\hat{d} = 2 \cdot 10^{-4}$, $|\phi_o| = 10^{-4}$, 2 - $\hat{d} = 2 \cdot 10^{-4}$, $|\phi_o| = 3 \cdot 10^{-4}$, 3 - $\hat{d} = 2 \cdot 10^{-4}$, $|\phi_o| = 2 \cdot 10^{-3}$. The horizontal line segments for each curve correspond to the refraction by the angle $\theta_L = \sqrt{|\phi_o|}$. The widths of these segments correspond to the spiral-scattering and deflection boundaries.

rapidly up to the maximum for $|\phi_o| \approx 3|\phi_{o,c}|$ and then decreases to zero. In this specific case, the normalized maximum value $\Delta\hat{b}_{s,max}/(\hat{d}/2)$ is $\approx 19\%$ of the width $\hat{d}/2$ (see Fig. 2) and its distance from the critical energy is $|\phi_o|/|\phi_{o,c}|$. Thus, the position of the maximum on this scale is independent of the particle energy. Moreover, the normalized width

$$\Delta\hat{b}_s/(\hat{d}/2) = f(|\phi_o|/|\phi_{o,c}|) \quad (24)$$

is a universal function determined only by the shape of the potential. At the same time, the value of the parameter $|\phi_o|$ for which the maximum is reached evidently depends on the particle energy. However, the above-mentioned scaling invariance holds in this case. This feature is seen in Fig. 4, which presents the width of the spiral-scattering range for the ring potential given by Eq. (1) with the hollow core ($U(r) = 0$ for $r < R - d/2$). This potential ensures maximum volume reflection in comparison with other ring potentials of the depth U_0 and width d constructed of two inversed parabolas. Thus, this potential provides a minimum estimate for the possible width of spiral scattering for an actual crystal. The value $\Delta\hat{b}_{s,max}/(\hat{d}/2) \approx 7\%$ and position $|\phi_o|/|\phi_{o,c}| \approx 1.3$ of the maximum of the spiral scattering width are different in this case, but the scaling invariance holds.

Note that the $\alpha(\hat{b})$ plots for \hat{d} and $|\phi_o|$ values other than those shown in Fig. 3 have the same form if α and \hat{b} are normalized to θ_L and $\hat{d}/2$, respectively, due to the above mentioned scaling invariance. It is seen that the width of the spiral-scattering range for large $|\phi_o|$ values ($|\phi_o| = 20 \cdot |\phi_{o,c}|$, curve 3 for the relatively low energies) decreases and tends to zero in the limit. In this case,

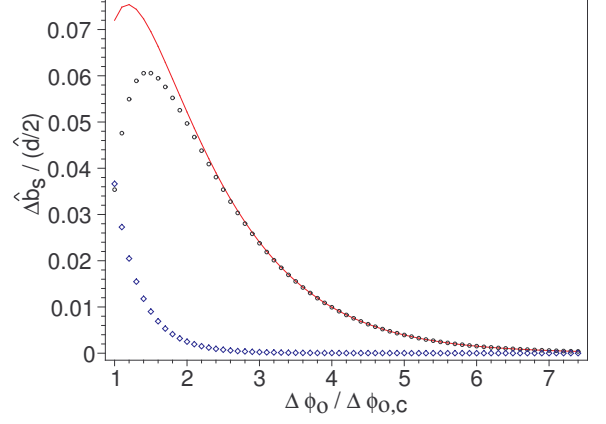


FIG. 4: Solid curve is the dimensionless spiral-scattering width $\Delta\hat{b}_s/(\hat{d}/2)$ calculated numerically for the ring potential with a half-parabola by 18. The circles show the contribution from $\Delta\hat{b}_s$ to $\Delta\hat{b}_{sl}$. The diamonds show the contribution from $\Delta\hat{b}_{sl}$ to $\Delta\hat{b}_{sr}$.

the deflection function tends to Eq. (13) for the square-well scattering, for which the smoothness of the edge is not important and the deflection angles $\alpha(\hat{b})$ are no larger than θ_L (the angle $\chi(\hat{b})$ is no larger than $2\theta_L$). The width of the spiral-scattering range, $\Delta\hat{b}_s$, increases with energy (with decreasing $|\phi_o|$). This width on curve 2 is maximal for $|\phi_o| = 3|\phi_{o,c}|$. Then, the width $\Delta\hat{b}_s$ decreases. Curve 1 corresponds to the critical energy $|\phi_o| = |\phi_{o,c}| = \hat{d}/2$, for which channeling is already impossible since the effective well is absent. Meanwhile, spiral scattering exists for this energy.

The last feature is due to the existence of a singularity of the deflection function for any smooth periodic potential similar to that shown in Fig. 5 if the critical conditions corresponding to the equality in Eqs. (11) and (12) are exactly satisfied. However, in contrast to the logarithmic singularity considered by Ford and Wheeler [1] and given by expansion (6), the singularity type changes. In this case, an inflection point (P_c in Fig. 5) appears instead of the local minimum; i.e., the second derivative $u''(r_{min})$ is also zero at this point and the series expansion of $u(r)$ in the vicinity of the minimum $r = r_{min}$ becomes

$$u(r) \approx u(r_{min}) + \frac{u(r_{min})'''}{6}(r - r_{min})^3. \quad (25)$$

It is easy to see that integral (4) for $b = u(r_{min})$ has the inverse square-root singularity

$$\chi(b) \approx -\frac{1}{\sqrt{|u(r_{min}) - b|}}, \quad (26)$$

Hence, the spiral scattering and deflection should take place for $|\phi_o| = |\phi_{o,c}|$.

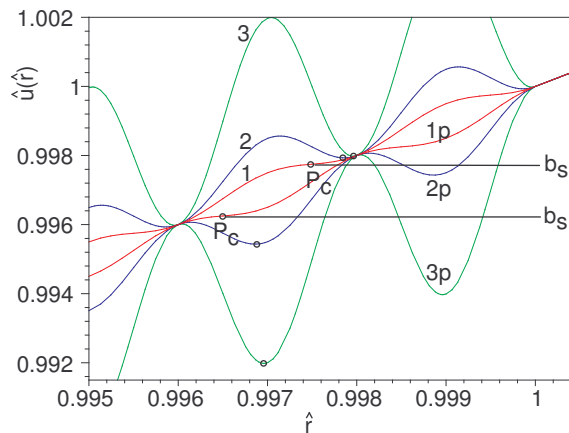


FIG. 5: Function $\hat{u}(\hat{r}) = \hat{r} \sqrt{1 \pm \frac{\phi_0(1 - \cos(2\pi(1 - \hat{r})/\hat{d}))}{2}}$ for a crystal potential for various particle energies and fixed parameters R, U_0, d . 1, 2, 3 - negatively charged particles with ($\hat{d} = 0.002, \phi_0 = 0.001, 0.003, 0.01$); 1p, 2p, 3p - positively charged particles (the minus sign under the square root in $\hat{u}(\hat{r})$); P_c are the inflection points of plots 1 and 1p for the critical energies corresponding to the Tsyanov criterion.

Note that although the effective force is zero at the local minimum and inflection points, the spiral scattering and deflection by a potential without the centrifugal term always take place at the internal slope of the potential responsible for attraction (see the local minima in Fig. 5).

These features hold also for a real crystal potential having one local minimum or inflection point per period under conditions (11) and (12). In this case, the position and maximum width are certainly different and, in addition, the width should be normalized to the crystal period \hat{d} . This yields the lower estimate for the maximum width $\Delta \hat{b}_s/\hat{d} \approx 3.5\%$ (ring potential) and the upper estimate $\Delta \hat{b}_s/\hat{d} \approx 9.5\%$ (potential with edge). However, the scaling invariance should also hold for these potentials.

For experiments, this means that if, e.g., the crystal curvature radius R is changed, then the particle energy E for a given crystal potential can always be chosen so that the parameter $|\phi_0|$ satisfies the criterion for which the spiral-scattering width is maximal. At the same time, the bending radius R maximizing the spiral-scattering width can always be pointed out for any relativistic particle energy E .

It should be noted that the multiple scattering and dissipation processes in a real crystal do not eliminate the singularity associated with spiral scattering. This was demonstrated for nuclear reactions such as, e.g., $^{40}\text{Ar} + ^{232}\text{Th}$, in which deep inelastic processes were interpreted in terms of negative spiral-scattering angles with allowance for friction forces [9]. This is explained by the fact that friction forces deform particle trajectories, but

the spiral-scattering range $\Delta \hat{b}_s$ remains unchanged.

Owing to the absence of thermal vibrations and the low electron density in the region of local minima, the volume capture of negatively charged particles is much smaller and the spiral-scattering width is much greater than the respective quantities for positively charged particles. Hence, negatively charged particles deflected along the crystal bending by an angle larger than $2\theta_L$ propagate in the spiral-scattering mode. The above estimates show that the fraction of negatively charged particles for the maximum spiral-scattering width is 3%–9%. The preliminary experiments [10, 11] on the scattering of 180-GeV electrons in *Si* show that a fairly large number of particles move at an angle larger than $> 2\theta_L = 32$ rad and do not have the peak typical of volume capture at the end of the angular size of the crystal.

The local minima in the case of positively charged particles moving in weakly bent crystals are in the region of high electron densities and thermal fluctuations of potentials. Thus, the trapping of spiral particles to the channeling mode seems to be the most probable secondary process. However, the spiral scattering is also significant in this case since the motion along the crystal bending ensures the intense volume capture of the particles in the region $\Delta \hat{b}_s$. For the crystal bending equal to the critical radius R_c when the channeled states are absent, the presence of particles with a rotation angle exceeding $2\theta_L$ can be undoubtedly interpreted as the presence of spiral scattering in this case and in the case of negatively charged particles.

I am grateful to Andrea Mazzolari for attracting my attention to work [10].

-
- [1] K. W. Ford and J. A. Wheeler. *Annals of Physics*, 7, 259–286, (1959).
 - [2] M. V. Berry and K.E. Mount. *Rep. Prog. Phys.*, 35, 315–397, (1972).
 - [3] N. P. Kalashnikov and G. V. Kovalev. *JETP Letters*, 29(6), 302–307, (1979).
 - [4] G. V. Kovalev. *JETP Letters*, 87(2), 94–98, (2008).
 - [5] G. V. Kovalev. *JETP Letters*, 87(7), 349–353, (2008).
 - [6] L. D. Landau and E. M. Lifshitz. *Mechanics (Course of Theoretical Physics, Volume 1)*. Butterworth-Heinemann; 3rd edition, NY, (1976).
 - [7] A. M. Taratin and S. A. Vorobiev. *Phys. Lett., A* 119(8), 425–428, (1987).
 - [8] J. Borwein, D. Bailey, and R. Girgensohn. *Experimentation in Mathematics. Computational Paths to Discovery*. A K Peters, Natick, Massachusetts, (2004).
 - [9] J. Wilczynski. *Phys. Lett.*, 47B(6), 484–486, (1973).
 - [10] W Scandale. *Overview of H8RD22 CERN Results. Presentation, FNAL*, page 32, (06.12.2007).
 - [11] W Scandale. *Bent Crystals in LHC. For UA9 collaboration, Erice*, page 26, (29.10.2008).